Ozone pollution in the North China Plain spreading into the late-winter haze season

Ke Li[a,b], Daniel J. Jacob[b,1], Hong Liao[c,1], Yulu Qiu[d], Lu Shen[b], Shixian Zhai[b], Kelvin H. Bates[b], Melissa P. Sulprizio[b], Shaojie Song[b], Xiao Lu[b], Qiang Zhang[e], Bo Zheng[f], Yuli Zhang[g], Jinqiang Zhang[g], Hyun Chul Lee[h], and Su Keun Kuk[h]

[a]Harvard–NUIST Joint Laboratory for Air Quality and Climate, Nanjing University of Information Science and Technology, 210044 Nanjing, China; [b]John A. Paulson School of Engineering and Applied Sciences, Harvard University, Cambridge, MA 02138; [c]Jiangsu Key Laboratory of Atmospheric Environment Monitoring and Pollution Control, Collaborative Innovation Center of Atmospheric Environment and Equipment Technology, School of Environmental Science and Engineering, Nanjing University of Information Science and Technology, 210044 Nanjing, China; [d]Environmental Meteorology Forecast Center of Beijing-Tianjin-Hebei, Beijing 100089, China; [e]Department of Earth System Science, Tsinghua University, 100084 Beijing, China; [f]Institute of Environment and Ecology, Tsinghua Shenzhen International Graduate School, Tsinghua University, Shenzhen 518055, China; [g]Key Laboratory of Middle Atmosphere and Global Environment Observation, Institute of Atmospheric Physics, Chinese Academy of Sciences, Beijing 100029, China; and [h]Samsung Advance Institute of Technology, Suwon-si, Gyeonggi-do, 16678, Republic of Korea

Edited by Guy P. Brasseur, Max Planck Institute for Meteorology, Hamburg, Germany, and accepted by Editorial Board Member Akkihebbal R. Ravishankara January 30, 2021 (received for review July 26, 2020)

Surface ozone is a severe air pollution problem in the North China Plain, which is home to 300 million people. Ozone concentrations are highest in summer, driven by fast photochemical production of hydrogen oxide radicals (HO_x) that can overcome the radical titration caused by high emissions of nitrogen oxides (NO_x) from fuel combustion. Ozone has been very low during winter haze (particulate) pollution episodes. However, the abrupt decrease of NO_x emissions following the COVID-19 lockdown in January 2020 reveals a switch to fast ozone production during winter haze episodes with maximum daily 8-h average (MDA8) ozone concentrations of 60 to 70 parts per billion. We reproduce this switch with the GEOS-Chem model, where the fast production of ozone is driven by HO_x radicals from photolysis of formaldehyde, overcoming radical titration from the decreased NO_x emissions. Formaldehyde is produced by oxidation of reactive volatile organic compounds (VOCs), which have very high emissions in the North China Plain. This remarkable switch to an ozone-producing regime in January–February following the lockdown illustrates a more general tendency from 2013 to 2019 of increasing winter–spring ozone in the North China Plain and increasing association of high ozone with winter haze events, as pollution control efforts have targeted NO_x emissions (30% decrease) while VOC emissions have remained constant. Decreasing VOC emissions would avoid further spreading of severe ozone pollution events into the winter–spring season.

wintertime ozone | air quality | haze season | China | emission control

China is beset by both cold-season particulate pollution (winter haze) and warm-season surface ozone pollution (1, 2). The worst conditions are in the North China Plain, home to over 300 million residents, where wintertime $PM_{2.5}$ (particulate matter smaller than 2.5 μm in diameter) and summertime ozone concentrations routinely exceed air quality standards (3–6). Vigorous emission controls implemented by the Chinese government through the Clean Air Action (7) have reduced $PM_{2.5}$ concentrations in the North China Plain by 40 to 50% since 2013 for all seasons (8), but summertime ozone concentrations have been increasing (9). Ozone is generally viewed as a summertime problem, with very low concentrations in winter (4, 10). Here, we show that the emission reductions under the Clean Air Action have actually extended the ozone pollution season in the North China Plain into winter–spring, and we present evidence from the coronavirus disease 2019 (COVID-19) shutdown of January–February 2020 that fast ozone production can take place in the North China Plain in winter as emissions decrease.

Ozone production takes place in polluted regions by photochemical oxidation of volatile organic compounds (VOCs) in the presence of nitrogen oxides ($NO_x \equiv NO + NO_2$), catalyzed by hydrogen oxide radicals ($HO_x \equiv OH$ + peroxy radicals) as oxidants. NO_x in urban air is mainly from fossil fuel combustion, while VOCs have a range of anthropogenic sources. The major sources of HO_x radicals in urban air are the ultraviolet (UV) photolysis of ozone, nitrous acid (HONO), formaldehyde (HCHO), and other carbonyl compounds (11–13). The ozone pollution season at northern midlatitudes is typically limited to May–September months when UV fluxes are high (5, 14). However, high ozone events in winter have been observed in an oil/gas production basin in the United States and attributed to photolysis of carbonyls with HCHO as the leading species (12, 15). Ozone production in winter is generally in the VOC-limited regime (equivalently called the NO_x-saturated regime) because of radical scavenging from oxidation of NO_x to nitric acid (16). Thus, ozone is expected to increase as VOC emissions increase and as NO_x emissions decrease.

Photolysis of HONO is a large source of HO_x radicals in the North China Plain in winter (13, 17, 18). However, winter ozone

Significance

The North China Plain experiences severe summer ozone pollution, but ozone during winter haze (particulate) pollution events has been very low. Here, we show that the abrupt decrease in nitrogen oxide (NO_x) emissions following the COVID-19 lockdown in January 2020 drove fast ozone production during winter haze events to levels approaching the air quality standard. This fast ozone production was driven by formaldehyde originating from high emissions of volatile organic compounds (VOCs). The COVID-19 experience highlights a general 2013 to 2019 trend of rapidly increasing ozone pollution in winter–spring in China as NO_x emissions have decreased. VOC emission controls would mitigate the spreading of ozone pollution into winter–spring with benefits for public health, crop production, and particulate pollution.

Author contributions: K.L. and D.J.J. designed research; K.L. performed research; Y.Q., L.S., S.Z., K.H.B., M.P.S., Q.Z., B.Z., Y.Z., J.Z., H.C.L., and S.K.K. contributed new data/analytic tools; K.L., H.L., Y.Q., S.S., and X.L. analyzed data; K.L., D.J.J., and H.L. wrote the paper; and all authors contributed to discussing and improving the paper.

The authors declare no competing interest.

This article is a PNAS Direct Submission. G.P.B. is a guest editor invited by the Editorial Board.

[1]To whom correspondence may be addressed. Email: djacob@fas.harvard.edu or hongliao@nuist.edu.cn.

This article contains supporting information online at https://www.pnas.org/lookup/suppl/doi:10.1073/pnas.2015797118/-/DCSupplemental.

Published March 1, 2021.

concentrations are generally low (19), dropping down to a few parts per billion (ppb) during winter haze pollution episodes (20, 21) when weather conditions are stagnant (22, 23). Observations in the North China Plain show a strong negative correlation between $PM_{2.5}$ and ozone in winter (4, 24). The low ozone is attributed to titration by high NO emissions (19) and strong suppression of ozone formation under NO_x-saturated conditions (20).

The abrupt lockdown of the North China Plain on January 24, 2020, in response to COVID-19 led to a sharp decrease in NO_x emissions as indicated by ground-based and satellite data (25–27). Winter haze events with high $PM_{2.5}$ were still observed during the lockdown but were associated with increased ozone levels (28). The oxidizing environment resulting from the increased ozone was reported to be the driving reason for the high secondary $PM_{2.5}$ concentrations during the lockdown (29, 30). The increase of ozone during the lockdown has been tentatively attributed to weakened titration (29, 31), ozone production (32), and decreased $PM_{2.5}$ (27, 31). Understanding the factors controlling the high ozone observed in winter haze events during the lockdown provides insight into how continued decrease of emissions could result in growing ozone pollution in the North China Plain in winter–spring.

Here, we first present air quality observations in the North China Plain during the COVID-19 lockdown and show that fast photochemical ozone production took place in haze events. We show that the COVID-19 lockdown underscores what has been a general trend since 2013 of increasing ozone pollution in winter–spring, including exceedances of the air quality standard of 160 μg m^{-3} (75 ppb at Standard Temperature and Pressure [STP]) for the maximum daily 8-h average (MDA8) ozone concentration. We explain this increase as driven by the 30% decrease of NO_x emissions combined with flat VOC emissions for the 2013 to 2019 period under the Clean Air Action. Unlike in summer, we find that the ozone increase in winter–spring is not driven by decreasing $PM_{2.5}$ (6) but rather by decreasing NO_x emission. The decrease of NO_x emissions has caused a major broadening of the ozone pollution season to now extend over much of the year. The COVID-19 lockdown experience shows that high ozone events may become more frequent and severe in winter–spring in the absence of action to reduce VOC emissions.

Results and Discussion

High Ozone in Winter Haze during the COVID-19 Lockdown. The national lockdown policy starting on January 24, 2020, drove a sharp decrease in transportation and industrial emissions, amplified by the Chinese Spring Festival holiday. We define here the lockdown period as January 24 to February 15 when lockdown measures were particularly strict (25). Fig. 1 and *SI Appendix*, Fig. S1 show 60 to 70% observed decreases in surface NO_2 concentrations and tropospheric NO_2 columns from the TROPOspheric Monitoring Instrument (TROPOMI) satellite, implying sharp reductions of NO_x emissions. TROPOMI HCHO observations suggest a weaker reduction of VOC emissions. The surface NO_2 concentrations are from the Ministry of Ecology and the Environment (MEE) monitoring site network. For the North China Plain as defined in Fig. 1*A*, average decreases during the lockdown were 57% for surface NO_2, 67% for TROPOMI NO_2, and 13% for TROPOMI HCHO. By contrast, ozone concentrations measured at MEE sites increased substantially during the COVID-19 lockdown. Maximum MDA8 ozone at individual sites in the North China Plain increased from 41 ± 5 ppb before lockdown (Fig. 1*D*) to 59 ± 5 ppb during lockdown (Fig. 1*H*).

Fig. 2 shows the time series of MDA8 ozone, $PM_{2.5}$, and peroxyacetyl nitrate (PAN) in Beijing before and during the lockdown. Stagnant weather during the lockdown (29, 32) caused two severe haze episodes, as seen in the $PM_{2.5}$ peaks on January 28 and February 12. Ozone during these two events rose to 56 and 57 ppb, respectively, which positively correlated with $PM_{2.5}$. The correlation between ozone and $PM_{2.5}$ shifted from negative ($r = -0.53$, $P < 0.05$) before the lockdown to positive ($r = 0.52$, $P < 0.05$) during the lockdown. Data from previous years show persistent negative correlations between $PM_{2.5}$ and ozone in the wintertime in the North China Plain (4, 24). This is in contrast to summer when $PM_{2.5}$ and ozone are positively correlated except under very high $PM_{2.5}$ conditions (33). Odd oxygen ($O_x \equiv O_3 + NO_2$) increases during the two haze episodes (*SI Appendix*, Fig. S2), indicating that the increase of ozone is not simply attributable to decreased titration by NO emissions and must be driven instead by photochemical production.

Further evidence for photochemical production of ozone comes from the increase in PAN during the haze pollution events of the lockdown period, reaching up to 4 ppb and synchronous with ozone and $PM_{2.5}$ (Fig. 2*C*). By contrast, PAN levels were very low before lockdown. PAN is produced by the same photochemistry as ozone, and under polluted conditions, its production rate is determined by the HO_x source and the NO_2/NO ratio, the latter increasing with increasing ozone (34). Both ozone and PAN show diurnal cycles of depletion at night and increases in the daytime, with particularly large daytime increases during the haze episodes indicative of fast photochemical production (*SI Appendix*, Fig. S3).

We used the Goddard Earth Observing System Chemical Transport Model (GEOS-Chem) with 25-km resolution (*Materials and Methods*) to explain the high ozone in haze events during the COVID-19 lockdown. The model has been used previously to simulate $PM_{2.5}$ (35) and summertime ozone (33) in the North China Plain. Anthropogenic emissions are from the Multiresolution Emission Inventory for China (MEIC) (36) and updated to 2020 by applying sectoral scaling factors (*Materials and Methods*). The effect of the lockdown is simulated by decreasing NO_x and VOCs emissions by 60% and 30%, respectively, consistent with independent estimates (25, 29) and with the NO_2 and HCHO observations of Fig. 1 and *SI Appendix*, Fig. S1. This decreases mean NO_2 concentrations at MEE sites over the North China Plain by 69% in the model compared to 57% in the observations. Tropospheric NO_2 columns decrease by 71% in the model compared to 67% in the TROPOMI observations. Correcting the TROPOMI retrieval for the change in NO_2 vertical profile during the lockdown (*SI Appendix*, Fig. S4) implies a 68% decrease rather than 67%. Tropospheric HCHO columns decrease by 29% in the model compared to 13% in the observations and 17% in the observations corrected for the change in vertical profile (*SI Appendix*, Fig. S4). HCHO columns in the Beijing area actually show a mean increase during the lockdown, both in the model and the observations (*SI Appendix*, Fig. S1), reflecting the two aforementioned stagnation events with amplified oxidant chemistry as discussed below. A sensitivity model simulation indicates that NO_2 and HCHO columns over the North China Plain would have changed by −17% and +3%, respectively, over the 6-wk period if emissions had stayed constant.

We find that the model can reproduce the elevated $PM_{2.5}$, ozone, and PAN during the winter haze episodes in the lockdown period (Fig. 2). The sensitivity simulation with no decreases of NO_x and VOC emissions during the lockdown period underestimates ozone by 10 to 20 ppb (*SI Appendix*, Fig. S5). Fig. 2*D* shows the model sources of HO_x radicals driving the photochemistry. HONO is the dominant HO_x source before lockdown, consistent with previous observational (13, 17, 18) and model studies (37, 38). The source of HONO in GEOS-Chem is mainly from heterogeneous NO_2 chemistry (39–41) plus a minor direct emission from transportation (42) and is therefore greatly reduced during the lockdown, consistent with observations (43). We find, on average, a 54% decrease of HONO concentrations during the lockdown in the surface to 500-m column. The HONO photolysis rate increases by 19% during the lockdown, mainly due to changes in meteorology. Consequently, OH radical from the HONO photolysis decreases by 41% (Fig. 2*D*).

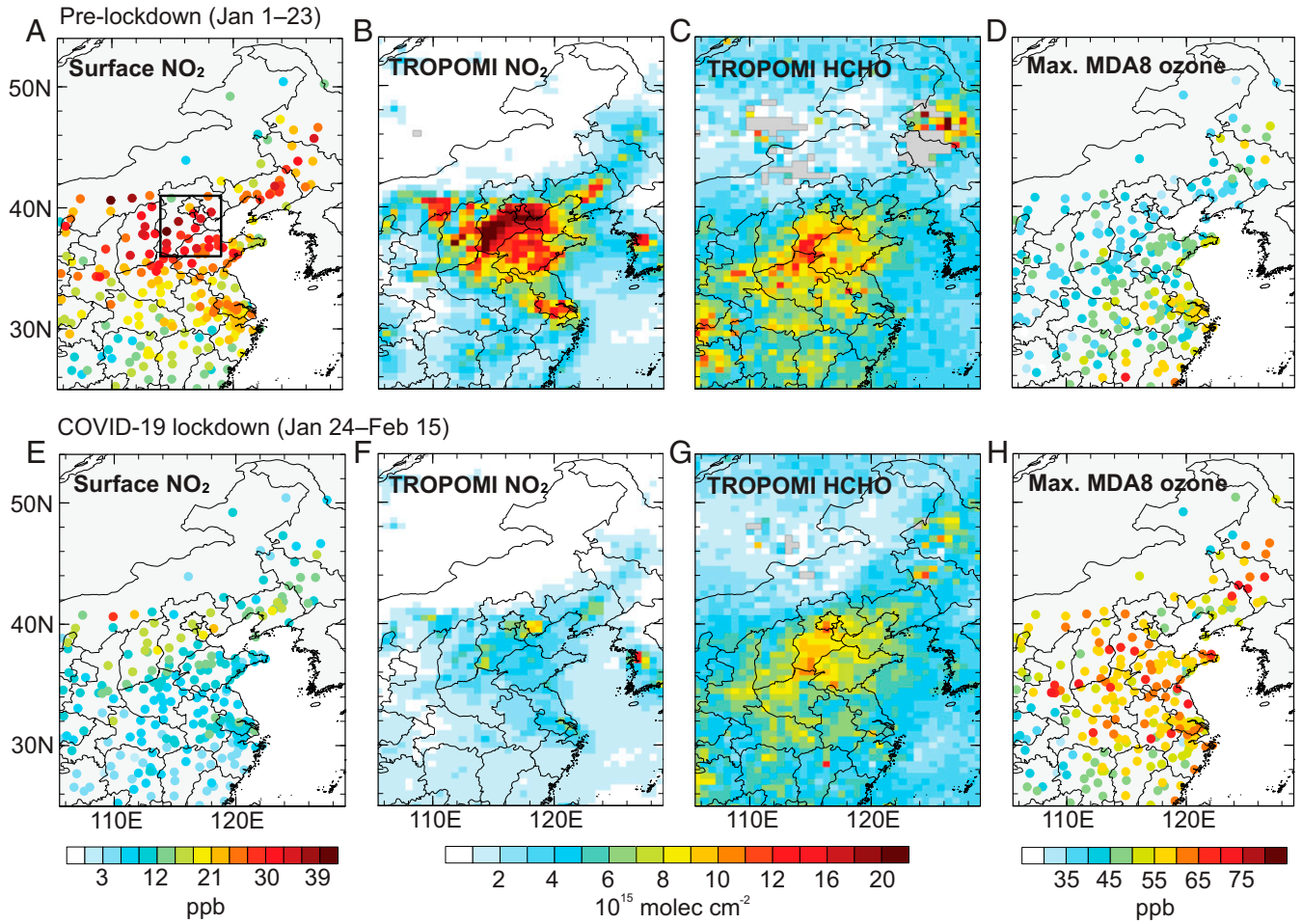

Fig. 1. COVID-19 lockdown impact on NO_x emissions, VOC emissions, and surface ozone concentrations. (*A*, *E*) Surface NO_2 concentrations averaged over the prelockdown (January 1 to 23, 2020) and COVID-19 lockdown (January 24 to February 15, 2020) periods at individual cities of the surface network operated by the China MEE. The black box delineates the North China Plain (36 to 41°N, 114 to 119°E) as defined in the text. There are 23 MEE network cities in the North China Plain. The concentrations are reported by the MEE in the unit of μg m^{-3} and were converted to ppb here (*Materials and Methods*). Tropospheric NO_2 (*B*, *F*) and HCHO (*C*, *G*) column densities measured by the TROPOMI satellite instrument during the prelockdown and lockdown periods. The TROPOMI data are aggregated on a 0.5° × 0.625° grid. (*D*, *H*) Maximum MDA8 ozone (ppb) over the prelockdown and lockdown periods as measured by the MEE surface network.

We find that the dominant HO_x source during the lockdown is the photolysis of HCHO, which is much larger than prelockdown period despite the decrease in VOC emissions. The HO_x source from HCHO photolysis is particularly large during the two haze events of January 28 and February 12, reflecting the stagnant conditions (*SI Appendix*, Fig. S6). The model includes primary HCHO emissions from the transportation and residential sectors (*Materials and Methods*), but we find that 95% of HCHO during lockdown is secondary from oxidation of VOCs. That fraction is 88% before lockdown, consistent with observational studies that find most of the HCHO in wintertime Beijing to be secondary (44, 45). Reactive alkenes and aromatics dominate the HCHO source and drive ozone production (*SI Appendix*, Fig. S7). We find in the model that HCHO acts as a photochemical amplifier whereby increased production of HCHO under stagnant weather conditions leads to higher OH concentrations and hence accelerates the oxidation of VOCs by OH. This radical amplification process combined with decreased NO_x emissions allows for fast ozone production. The faster oxidation of VOCs also drives large increases of PAN in the model.

Growing Ozone Pollution during the Winter Haze Season, 2013 to 2019. The experience of the COVID-19 lockdown dramatically illustrates how the continuing decrease of NO_x emissions in China under the Clean Air Action may lead to high-ozone episodes during the winter haze season. National NO_x emissions have decreased by 30% over the 2013 to 2019 period (9, 36, 46, 47). Fig. 3 shows an increasing trend of maximum MDA8 ozone in March from 2013 to 2019, demonstrating the growing northward spread of ozone pollution into the winter haze season, with extensive exceedances of the air quality standard. $PM_{2.5}$ decreases over the same period, but the daily correlation between $PM_{2.5}$ and ozone is increasingly positive (Fig. 3), implying fast ozone production with simultaneously elevated $PM_{2.5}$ during stagnant conditions. The same trend toward rapidly increasing ozone production from 2013 to 2019 is also observed in February (*SI Appendix*, Fig. S8), with ozone exceeding 75 ppb in the North China Plain by 2019 and the ozone–$PM_{2.5}$ correlation switching from negative to positive. Odd oxygen over the North China Plain in 2019 suggests an onset of ozone production in mid-February (*SI Appendix*, Fig. S2).

Fig. 4*A* shows the seasonality of observed 2013 to 2019 ozone trends in the North China Plain after filtering of interannual meteorological variability with a stepwise multiple regression model (*Materials and Methods*) to better resolve the effect of anthropogenic emission changes (6, 8, 9). Trends in the original unfiltered data are shown in *SI Appendix*, Fig. S9. We find that

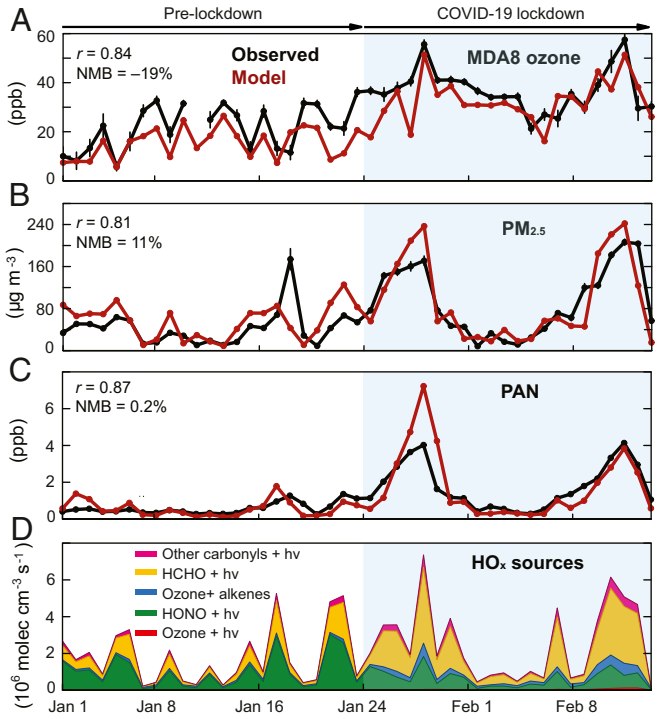

Fig. 2. Air quality changes in Beijing in response to the COVID-19 lockdown. (*A*–*C*) The black lines show observed concentrations of MDA8 ozone, 24-h average $PM_{2.5}$, and 24-h average PAN. The ozone and $PM_{2.5}$ observations are averages across the 12 Beijing monitoring sites of the MEE. The vertical bars in *A* and *B* are standard errors (SEs) on those averages. The PAN observations were made at Minzu University of China in urban Beijing (39.95°N, 116.32°E). Also shown are GEOS-Chem model results sampled at the same locations and the corresponding correlation coefficients (*r*) and normalized mean bias (NMB) relative to observations. (*D*) The GEOS-Chem sources of HO_x in Beijing averaged over the boundary layer (taken here as surface to 500-m altitude).

the ozone increase is largest in March and that the increase in February is comparable to that in summer. Fig. 4*B* shows the change in the observed frequency of ozone exceedances of the 160 μg m^{-3} air quality standard (days $month^{-1}$) for individual months between 2014 to 2016 and 2017 to 2019 for the 22 cities in the North China Plain with full records over the 6-y period. Exceedances are not yet observed in February, but exceedances in March rose to 2 days $month^{-1}$ in the 2017 to 2019 period.

We conducted GEOS-Chem simulations with 2013 and 2019 emissions to understand the effect of changes in anthropogenic emissions on the seasonality of ozone increase in the North China Plain (*Materials and Methods*). NO_x emissions in the MEIC inventory for the North China Plain decreased by 30% from 2013 to 2019, VOC emissions stayed flat, and observed $PM_{2.5}$ concentrations decreased by about 50% in all seasons (8, 9, 36). Model results shown in Fig. 4*A* indicate that these changes led to ozone increases in all months of the year, peaking in spring and fall. We previously found in GEOS-Chem that the $PM_{2.5}$ decrease was the principal driver for the ozone increase in summer due to decreased scavenging of HO_2 radicals assuming a reactive uptake coefficient of 0.2 (6, 33). Here, we reproduce this result and find that the ozone trend in July would have been negative if not for the $PM_{2.5}$ decrease. However, we also find that the $PM_{2.5}$ effect is largely limited to summer. In other seasons, oxidation of NO_x to nitric acid is the dominant HO_x sink (*SI Appendix*, Fig. S10). This explains the maximum ozone increases in the model in spring and fall when photochemistry is active but strongly VOC-limited (16).

The model underestimates the observed ozone increase in all seasons except in the fall. The MEE sites are generally located in urban centers, where VOC-limited conditions are strongest and may not be captured at the 25-km resolution of GEOS-Chem (6, 48). Similarly, wintertime increases in ozone due to decreased local titration by NO emissions would not be well represented at the 25-km model scale. There is additional uncertainty in the HO_2 reactive uptake coefficient and how it may vary with $PM_{2.5}$ composition (49). The model underestimate of the springtime trend may reflect an increase in background ozone, which is particularly important in that season (50). Ozonesonde measurements over the 2013 to 2018 period in Beijing (51) show an increase in free tropospheric ozone in spring but not in other seasons (*SI Appendix*, Fig. S11), which may be due to rising anthropogenic emissions in South and Southeast Asia (52).

Implications for Air Pollution Control. The extension of the ozone pollution season into winter–spring is observed not only for the North China Plain but across China (*SI Appendix*, Fig. S12). Regulatory attention has so far focused on summertime ozone pollution (53), but we find that the rate of ozone increase is larger in February to May months and that exceedances of the air quality standard can already occur as early as March in the North China Plain. Ozone is rapidly becoming a year-round air pollution problem in China, and one may expect more frequent occurrences of joint ozone–$PM_{2.5}$ pollution episodes. For example, a pollution event with MDA8 ozone of 140 ppb and 24-h $PM_{2.5}$ of 100 μg m^{-3} averaged over all Beijing MEE sites was observed on April 30 to May 1, 2020. Beyond public health, this broadening of the ozone pollution season threatens crop production (54), particularly for the spring growth of winter wheat in North China, which accounts for two-thirds of China's total wheat yield (55).

The fast increase of ozone and HO_x radicals outside of summer would stimulate the formation of secondary $PM_{2.5}$, including nitrate, sulfate, and organic components. Long-term $PM_{2.5}$ composition measurements in Beijing show an increase in the contributions of secondary species to total $PM_{2.5}$ (30, 56). Increased production of secondary $PM_{2.5}$ has been blamed for the occurrence of haze pollution episodes during the COVID-19 lockdown (29).

This rapid broadening of the ozone pollution season in China can be explained by the fast decrease of NO_x emissions combined with very high and flat VOC emissions. VOC oxidation produces carbonyls, in particular HCHO, whose photolysis produces HO_x radicals that drive fast ozone production and accelerate further VOC oxidation. This process has been previously reported to occur in oil/gas fields in the United States in winter (12), and here we see that it operates in urban China as well. Increasing background ozone in spring (51, 52, 57) could also contribute to the increase in surface ozone pollution.

NO_x emission controls in China have been motivated mainly by the goal of decreasing nitrate $PM_{2.5}$, and further controls are expected in the future (http://env.people.com.cn/n1/2020/0515/c1010-31710781.html). The Chinese government has recently announced controls on VOC emissions in June to September months in order to decrease ozone pollution (53). Our results suggest that extending these VOC emission controls year round would avoid further spread of ozone pollution outside the summer season.

In summary, we have found that winter haze episodes in the North China Plain following the COVID-19 lockdown in January 2020 featured fast photochemical production of ozone with concentrations reaching 60 to 70 ppb. This can be explained by the sharp decrease in NO_x emissions combined with high VOC emissions, driving ozone production through HCHO photolysis. This rapid ozone production during the COVID-19 winter haze episodes in January to February illustrates a more general trend from 2013 to 2019 of increasing ozone pollution in winter–spring, driven by a 30% decrease of NO_x emissions while VOC emissions

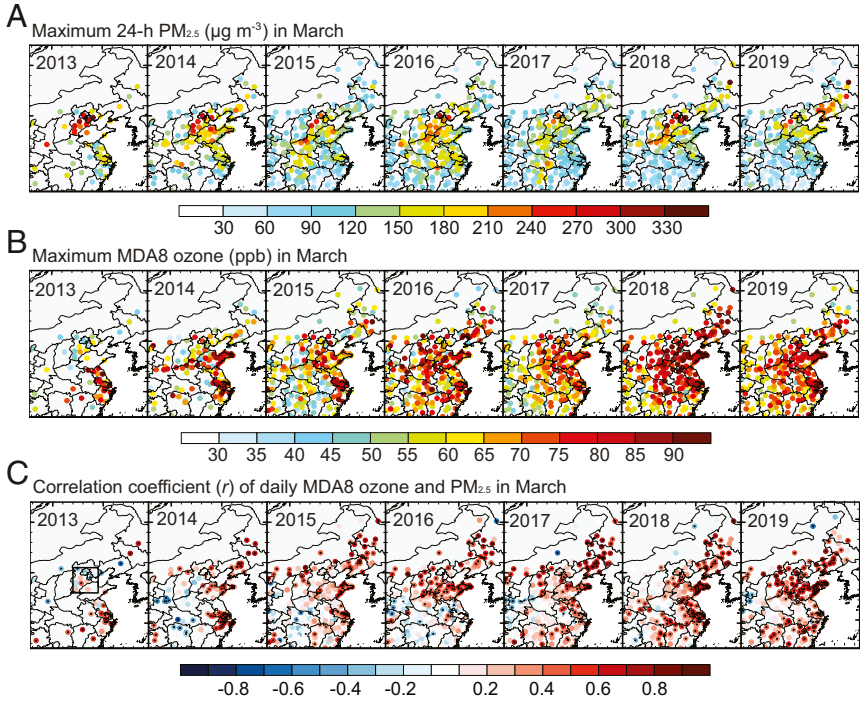

Fig. 3. Growing ozone pollution in the winter haze season, 2013 to 2019. The concentration data are from the network operated by the China MEE since 2013 and are shown here for March of individual years. (*A*) Maximum 24-h $PM_{2.5}$. (*B*) Maximum MDA8 ozone. (*C*) Pearson correlation coefficients (*r*) of daily MDA8 ozone and 24-h $PM_{2.5}$. The dots indicate correlation coefficients that are statistically significant above the 95% confidence level. The black box (*Bottom Left*) delineates the North China Plain as defined in the text. *SI Appendix*, Fig. S8 shows the same results for February.

have stayed flat. Curbing ozone pollution in China will require VOC emission controls year round as NO_x emissions continue to decrease. Such controls will benefit not just the North China Plain but also the country as a whole.

Materials and Methods

Observations. Surface hourly concentrations of ozone, $PM_{2.5}$, and CO concentrations are reported by the MEE at a network that started from ~450 sites in 2013 and grew to ~1,500 sites by 2020 and included about 360 cities. We accessed the data through http://beijingair.sinaapp.com. We computed MDA8 ozone concentrations and 24-h average concentrations for other air pollutants from the hourly data for the 2013 to 2020 period. The reported concentrations are in the unit of μg m^{-3} for gas species under standard conditions of temperature and pressure (STP; 273 K, 1,013 hPa) until August 31, 2018. This reference state was changed to (298 K, 1,013 hPa) on September 1, 2018. We converted concentrations to ppb following ref. 9. We also used PAN concentrations measured by researchers from the China Meteorological Administration at a site on the campus of Minzu University of China (39.95°N, 116.32°E) in urban Beijing. The measurements were made with an online gas chromatograph equipped with an electron capture detector (58).

Satellite observations of NO_2 (59) and HCHO (60) columns from the TROPOMI instrument were accessed from https://s5phub.copernicus.eu/dhus/. TROPOMI provides daily global coverage with 5.5 × 3.5 km^2 pixel resolution. TROPOMI data have been applied in tracking anthropogenic emission changes during the lockdown (26, 61). We used the TROPOMI Level 2 observations with quality assurance values larger than 0.75 for NO_2 (version 1.3.2) and larger than 0.5 for HCHO (version 1.1.8).

Chemical Transport Model Simulations.

GEOS-Chem model description. We simulated air quality over China by using the GEOS-Chem atmospheric chemistry model (version 12.7.1; http://www.geos-chem.org/). The model includes detailed ozone–NO_x–VOC–aerosol–halogen tropospheric chemistry (62, 63) and is driven by NASA GEOS-FP (Forward Processing) meteorological data (64) with 0.25° × 0.3125° horizontal resolution. We use that native resolution over a nested eastern China domain (30 to 45°N; 108 to 125°E). Chemical boundary conditions at the edges of the nested domain are updated every 3 h from a global simulation with 4° × 5° resolution.

The GEOS-Chem simulation of ozone pollution over China has been evaluated in a number of recent studies (6, 50, 65). Our model configuration largely follows that of ref. 33, but we use a higher spatial resolution. The standard GEOS-Chem model includes HONO and HCHO formed from NO_2 heterogeneous chemistry and VOC oxidation, respectively (39, 66). Here, we added HONO emissions from transportation by applying a HONO/NO_x emission ratio of 1.7% following ref. 42, and we multiplied transportation HCHO emissions in the standard model by a factor of 5 for the cold season (November to March) following refs. 67 and 48. These direct emissions made minor contribution to HONO and HCHO as compared to chemical production.

2013 to 2019 simulations. To quantify the effect of changing 2013 to 2019 emissions on ozone, we performed a set of simulations with fixed meteorology (September 2018 to August 2019) and perturbed emissions, using 6 mo of initialization. Anthropogenic emissions over China are from the MEIC, including seasonal (month-to-month) variability (36). MEIC emissions are available for the 2013 to 2017 period and were accessed from http://www.meicmodel.org. NO_x and SO_2 emissions for the 2017 to 2019 period were scaled on the basis of national emission trends reported by the MEE (46, 47). CO and $PM_{2.5}$ primary emissions for the 2017 to 2019 period were scaled on the basis of the MEE network data. In our nested eastern China domain, the decreases of emissions from 2013 to 2017 and from 2017 to 2019 are, respectively, 23% and 8% for NO_x, 62% and 11% for SO_2, 27% and 13% for CO, and 34% and 15% for $PM_{2.5}$. Anthropogenic emissions of ammonia (mainly from agriculture) and VOCs show no significant trend from 2013 to 2017 in the MEIC inventory. The lack of trend in VOC emissions is consistent with satellite HCHO data over eastern China showing no significant trend over the 2013 to 2019 period (9). Thus, we assume constant anthropogenic emissions of ammonia and VOCs from 2017 to 2019.

Simulations with Chinese anthropogenic emissions for years 2013 and 2019 were conducted to compute the 2013 to 2019 ozone trend in different months due to anthropogenic emission changes. A sensitivity simulation changing only anthropogenic NO_x and VOC emissions was also conducted to isolate the effect of $PM_{2.5}$ changes (33) by difference.

Effect of COVID-19 lockdown. To simulate ozone changes caused by the COVID-19 lockdown starting on January 24, 2020, we conducted GEOS-Chem simulations from January 1, 2020, to February 15, 2020, after 3 mo of initialization,

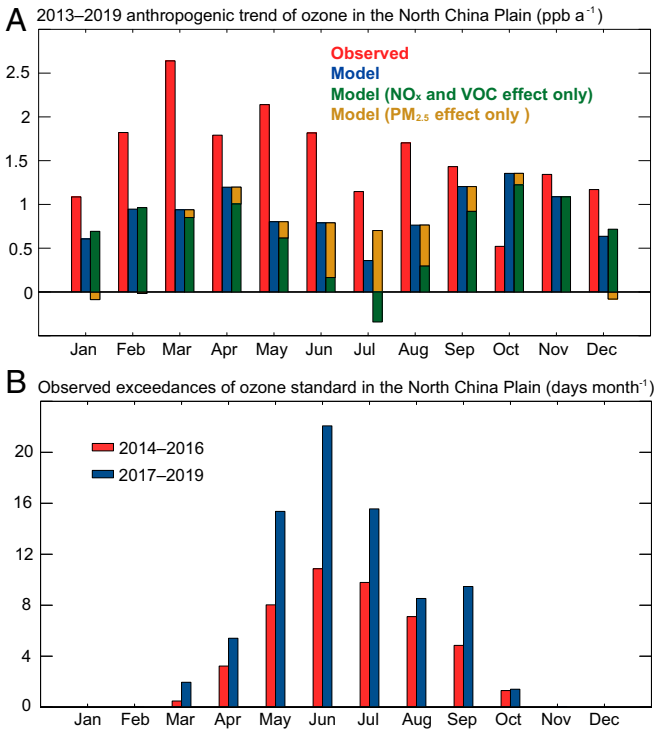

Fig. 4. Extension of ozone pollution season over the North China Plain into winter–spring, 2013 to 2019. (*A*) Anthropogenic trends of mean MDA8 ozone in individual months of the year. The observed anthropogenic trend is calculated by linear regression on the monthly mean values at MEE sites after removing the effect of interannual meteorological variability with a multiple linear regression model (6). The GEOS-Chem model trend is obtained by subtraction of results from simulations with 2013 and 2019 emissions, both using the same September 2018 to August 2019 meteorology. The $PM_{2.5}$ effect (33) is isolated in the model by removing the effect of changes in NO_x and VOC emissions. See *Materials and Methods* for more details. All observed ozone trends are statistically significant at the 95% confidence level, except for July and November, which have *P* values of 0.07 and 0.06, respectively. (*B*) The number of days per month with observed MDA8 ozone above the air quality standard (160 μg m^{-3}, corresponding to 75 ppb at STP), averaged over the 2014 to 2016 and 2017 to 2019 periods for the 22 MEE network cities in the North China Plain with full 2014 to 2019 records.

with the same model settings as the 2013 to 2019 simulations. Prelockdown anthropogenic emissions before January 24 were scaled from 2019 by extending the rate of 2017 to 2019 reductions to 2020. Relative to the prelockdown period, NO_x and VOC emissions over the simulation domain were reduced by 60% and 30%, respectively. This was done by applying reduction ratios of 90% for transportation emissions, 20% for power plants, 60% for industry (20% decrease for VOC emissions), and no changes for the residential and agriculture sectors. These reduction ratios are estimated from economic data in January to February of 2020 (68) and are consistent with the surface and satellite data for NO_2 and HCHO shown in Fig. 1 and *SI Appendix*, Fig. S1. Other studies have estimated emission reductions of 50 to 60% for NO_x and 30 to 40% for VOCs during the lockdown period (25, 29). We apply the emission reductions from January 24 to February 15 when the lockdown policy was most severe (25, 29, 32). The sector-based reductions also result in model emission decreases for SO_2, CO, and $PM_{2.5}$ of 40%, 39%, and 22%, respectively. Mean photolysis rates of NO_2, HONO, and HCHO in the surface to 500-m model column increased, respectively, by 19%, 19%, and 24% between January 1 to 23 and January 24 to February 15, mainly reflecting changes in meteorology.

To quantify the contribution of major VOC classes to HCHO and ozone production, we conducted sensitivity simulations with emissions for each of the five VOC groups (alkanes, alkenes, aromatics, HCHO, and other oxygenated VOCs) turned off separately in January to February of 2020. To quantify the role of meteorology in driving air quality change during the lockdown, a sensitivity simulation with no emission reductions was conducted.

Removing Meteorological Influence on Ozone Trends. To isolate the role of anthropogenic emission changes in driving 2013 to 2019 ozone trends, we removed the effect of interannual meteorological variability by using the stepwise multiple linear regression (MLR) model following refs. 6 and 9. Nine meteorological variables from the Modern-Era Retrospective analysis for Research and Applications, version 2 (MERRA-2) database (69), including temperature, 10-m zonal and meridional wind speed, 850-hPa meridional wind speed, relative humidity, boundary layer height, cloud cover, rainfall, and sea level pressure (6), were considered as candidate ozone covariates on the 0.5° × 0.625° MERRA-2 grid. We applied the MLR model to fit the day-to-day variability of MDA8 ozone independently for each site and each season. To avoid overfitting, only the three locally dominant meteorological parameters were regressed onto the final fit for the meteorologically-driven 2013 to 2019 trend in monthly MDA8 ozone. The residual trend was then taken to reflect the role of anthropogenic emissions following refs. 6 and 9.

Data Availability. The measurements, GEOS-Chem model code, and reanalysis data in this study are publicly available for download. Surface measurements of hourly air pollutants from China's MEE sites can be downloaded from http://beijingair.sinaapp.com. The TROPOMI satellite data can be freely accessed from https://s5phub.copernicus.eu/dhus/. The anthropogenic emission inventory is available from http://www.meicmodel.org. The GEOS-Chem model code is open source (https://doi.org/10.5281/zenodo.3676008). All other study data are included in the article and/or *SI Appendix*.

ACKNOWLEDGMENTS. This work is a contribution from the Harvard–NUIST Joint Laboratory for Air Quality and Climate. We acknowledge additional support from the Samsung Advanced Institute of Technology. We thank China's MEE for running the nationwide observation network and publishing hourly concentrations of air pollutants. We thank Yi Wang (The University of Iowa) for helpful discussion. H.L. is supported by National Natural Science Foundation of China Grants 42021004 and 91744311. K.L. is supported by National Natural Science Foundation of China Grant 41977191.

1. Z. An *et al.*, Severe haze in northern China: A synergy of anthropogenic emissions and atmospheric processes. *Proc. Natl. Acad. Sci. U.S.A.* **116**, 8657–8666 (2019).
2. T. Wang *et al.*, Ozone pollution in China: A review of concentrations, meteorological influences, chemical precursors, and effects. *Sci. Total Environ.* **575**, 1582–1596 (2017).
3. R. J. Huang *et al.*, High secondary aerosol contribution to particulate pollution during haze events in China. *Nature* **514**, 218–222 (2014).
4. Y. Wang, Q. Ying, J. Hu, H. Zhang, Spatial and temporal variations of six criteria air pollutants in 31 provincial capital cities in China during 2013-2014. *Environ. Int.* **73**, 413–422 (2014).
5. X. Lu *et al.*, Severe surface ozone pollution in China: A global perspective. *Environ. Sci. Technol. Lett.* **5**, 487–494 (2018).
6. K. Li *et al.*, Anthropogenic drivers of 2013-2017 trends in summer surface ozone in China. *Proc. Natl. Acad. Sci. U.S.A.* **116**, 422–427 (2019).
7. Chinese State Council, Action Plan on Air Pollution Prevention and Control (in Chinese). http://www.gov.cn/zwgk/2013-09/12/content_2486773.htm. Accessed 1 July 2020.
8. S. X. Zhai *et al.*, Fine particulate matter ($PM_{2.5}$) trends in China, 2013-2018: Separating contributions from anthropogenic emissions and meteorology. *Atmos. Chem. Phys.* **19**, 11031–11041 (2019).
9. K. Li *et al.*, Increases in surface ozone pollution in China from 2013 to 2019: Anthropogenic and meteorological influences. *Atmos. Chem. Phys.* **20**, 11423–11433 (2020).
10. M. Gao *et al.*, Ozone pollution over China and India: Seasonality and sources. *Atmos. Chem. Phys.* **20**, 4399–4414 (2020).
11. R. Volkamer, P. Sheehy, L. T. Molina, M. J. Molina, Oxidative capacity of the Mexico city atmosphere-Part 1: A radical source perspective. *Atmos. Chem. Phys.* **10**, 6969–6991 (2010).
12. P. M. Edwards *et al.*, High winter ozone pollution from carbonyl photolysis in an oil and gas basin. *Nature* **514**, 351–354 (2014).
13. Z. F. Tan *et al.*, Wintertime photochemistry in Beijing: Observations of RO_x radical concentrations in the North China Plain during the BEST-ONE campaign. *Atmos. Chem. Phys.* **18**, 12391–12411 (2018).
14. K. L. Chang *et al.*, Regional trend analysis of surface ozone observations from monitoring networks in eastern North America, Europe and East Asia. *Elem. Sci. Anth.* **5**, 1–50 (2017).
15. R. C. Schnell *et al.*, Rapid photochemical production of ozone at high concentrations in a rural site during winter. *Nat. Geosci.* **2**, 120–122 (2009).
16. D. J. Jacob *et al.*, Seasonal transition from NO_x- to hydrocarbon-limited ozone production over the eastern United States in September. *J. Geophys. Res.* **100**, 9315–9324 (1995).
17. X. Ma *et al.*, Winter photochemistry in Beijing: Observation and model simulation of OH and HO_2 radicals at an urban site. *Sci. Total Environ.* **685**, 85–95 (2019).
18. E. J. Slater *et al.*, Elevated levels of OH observed in haze events during wintertime in central Beijing. *Atmos. Chem. Phys.* **20**, 14847–14871 (2020).

19. H. Liu *et al*., Analysis of wintertime O_3 variability using a random forest model and high-frequency observations in Zhangjiakou-an area with background pollution level of the North China Plain. *Environ. Pollut.* **262**, 114191 (2020).
20. K. Lu *et al*., Fast photochemistry in wintertime haze: Consequences for pollution mitigation strategies. *Environ. Sci. Technol.* **53**, 10676–10684 (2019).
21. Y. Cheng *et al*., Reactive nitrogen chemistry in aerosol water as a source of sulfate during haze events in China. *Sci. Adv.* **2**, e1601530 (2016).
22. K. Li, H. Liao, W. Cai, Y. Yang, Attribution of anthropogenic influence on atmospheric patterns conducive to recent most severe haze over eastern China. *Geophys. Res. Lett.* **45**, 2072–2081 (2018).
23. X. Huang *et al*., Amplified transboundary transport of haze by aerosol–boundary layer interaction in China. *Nat. Geosci.* **13**, 428–434 (2020).
24. J. Zhu, L. Chen, H. Liao, R. J. Dang, Correlations between $PM_{2.5}$ and ozone over China and associated underlying reasons. *Atmosphere* **10**, 352 (2019).
25. R. X. Zhang *et al*., NO_x emission reduction and recovery during COVID-19 in east China. *Atmosphere* **11**, 433 (2020).
26. F. Liu *et al*., Abrupt decline in tropospheric nitrogen dioxide over China after the outbreak of COVID-19. *Sci. Adv.* **6**, eabc2992 (2020).
27. X. Shi, G. P. Brasseur, The response in air quality to the reduction of Chinese economic activities during the COVID-19 outbreak. *Geophys. Res. Lett.* **47**, e2020GL088070 (2020).
28. Y. Zhao *et al*., Substantial changes in nitrogen dioxide and ozone after excluding meteorological impacts during the COVID-19 outbreak in mainland China. *Environ. Sci. Technol. Lett.* **7**, 402–408 (2020).
29. X. Huang *et al*., Enhanced secondary pollution offset reduction of primary emissions during COVID-19 lockdown in China. *Natl. Sci. Rev.* **8**, 1–9 (2020).
30. Y. Sun *et al*., A chemical cocktail during the COVID-19 outbreak in Beijing, China: Insights from six-year aerosol particle composition measurements during the Chinese New Year holiday. *Sci. Total Environ.* **742**, 140739 (2020).
31. P. Sicard *et al*., Amplified ozone pollution in cities during the COVID-19 lockdown. *Sci. Total Environ.* **735**, 139542 (2020).
32. T. Le *et al*., Unexpected air pollution with marked emission reductions during the COVID-19 outbreak in China. *Science* **369**, 702–706 (2020).
33. K. Li *et al*., A two-pollutant strategy for improving ozone and particulate air quality in China. *Nat. Geosci.* **12**, 906–910 (2019).
34. E. V. Fischer *et al*., Atmospheric peroxyacetyl nitrate (PAN): A global budget and source attribution. *Atmos. Chem. Phys.* **14**, 2679–2698 (2014).
35. X. Wang *et al*., Effects of anthropogenic chlorine on $PM_{2.5}$ and ozone air quality in China. *Environ. Sci. Technol.* **54**, 9908–9916 (2020).
36. B. Zheng *et al*., Trends in China's anthropogenic emissions since 2010 as the consequence of clean air actions. *Atmos. Chem. Phys.* **18**, 14095–14111 (2018).
37. X. Fu *et al*., Persistent heavy winter nitrate pollution driven by increased photochemical oxidants in northern China. *Environ. Sci. Technol.* **54**, 3881–3889 (2020).
38. J. Zhang *et al*., Effect of potential HONO sources on peroxyacetyl nitrate (PAN) formation in eastern China in winter. *J. Environ. Sci. (China)* **94**, 81–87 (2020).
39. V. Shah *et al*., Effect of changing NO_x lifetime on the seasonality and long-term trends of satellite-observed tropospheric NO_2 columns over China. *Atmos. Chem. Phys.* **20**, 1483–1495 (2020).
40. F. Hendrick *et al*., Four years of ground-based MAX-DOAS observations of HONO and NO_2 in the Beijing area. *Atmos. Chem. Phys.* **14**, 765–781 (2014).
41. F. Meng *et al*., High-resolution vertical distribution and sources of HONO and NO_2 in the nocturnal boundary layer in urban Beijing, China. *Atmos. Chem. Phys.* **20**, 5071–5092 (2020).
42. J. Zhang, J. An, Y. Qu, X. Liu, Y. Chen, Impacts of potential HONO sources on the concentrations of oxidants and secondary organic aerosols in the Beijing-Tianjin-Hebei region of China. *Sci. Total Environ.* **647**, 836–852 (2019).
43. Y. Liu *et al*., Influence of Chinese new year overlapping COVID-19 lockdown on HONO sources in Shijiazhuang. *Sci. Total Environ.* **745**, 141025 (2020).
44. W. T. Chen *et al*., Understanding primary and secondary sources of ambient carbonyl compounds in Beijing using the PMF model. *Atmos. Chem. Phys.* **14**, 3047–3062 (2014).
45. J. Sheng *et al*., Characterizing the level, photochemical reactivity, emission, and source contribution of the volatile organic compounds based on PTR-TOF-MS during winter haze period in Beijing, China. *Atmos. Res.* **212**, 54–63 (2018).
46. Ministry of Ecology and Environment (MEE), Fulfillment of the annual goal of ecology environment protection (in Chinese). http://www.gov.cn/guowuyuan/2019-01/21/content_5359571.htm. Accessed 1 July 2020.
47. Ministry of Ecology and Environment (MEE), On the improvement of ecology and environment in 2019 by Minister (in Chinese). http://www.mee.gov.cn/ywdt/hjywnews/202001/t20200122_760857.shtml. Accessed 1 July 2020.
48. L. Jaeglé *et al*., Nitrogen oxides emissions, chemistry, deposition, and export over the Northeast United States during the WINTER aircraft campaign. *J. Geophys. Res.* **123**, 12368–12393 (2018).
49. J. Q. Mao, S. Fan, D. J. Jacob, Radical loss in the atmosphere from Cu-Fe redox coupling in aerosols. *Atmos. Chem. Phys.* **13**, 509–519 (2013).
50. R. J. Ni, J. T. Lin, Y. Yan, W. Lin, Foreign and domestic contributions to springtime ozone over China. *Atmos. Chem. Phys.* **18**, 11447–11469 (2018).
51. Y. L. Zhang *et al*., Long-term variations in ozone levels in the troposphere and lower stratosphere over Beijing: Observations and model simulations. *Atmos. Chem. Phys.* **20**, 13343–13354 (2020).
52. A. Gaudel *et al*., Aircraft observations since the 1990s reveal increases of tropospheric ozone at multiple locations across the Northern Hemisphere. *Sci. Adv.* **6**, eaba8272 (2020).
53. Ministry of Ecology and Environment (MEE), Solutions for control of volatile organic compounds (VOCs) in 2020 (in Chinese). http://www.mee.gov.cn/xxgk2018/xxgk/xxgk03/202006/t20200624_785827.html?from=timeline. Accessed 1 July 2020.
54. Z. Feng, E. Hu, X. Wang, L. Jiang, X. Liu, Ground-level O3 pollution and its impacts on food crops in China: A review. *Environ. Pollut.* **199**, 42–48 (2015).
55. C. Lu, L. Fan, Winter wheat yield potentials and yield gaps in the North China Plain. *Field Crops Res.* **143**, 98–105 (2013).
56. L. Lei *et al*., Long-term characterization of aerosol chemistry in cold season from 2013 to 2020 in Beijing, China. *Environ. Pollut.* **268**, 115952 (2021).
57. O. R. Cooper *et al*., Multi-decadal surface ozone trends at globally distributed remote locations. *Elem. Sci. Anth.* **8**, 1–23 (2020).
58. Y. Qiu, Z. Ma, K. Li, A modeling study of the peroxyacetyl nitrate (PAN) during a wintertime haze event in Beijing, China. *Sci. Total Environ.* **650**, 1944–1953 (2019).
59. J. van Geffen, H. J. Eskes, K. F. Boersma, J. D. Maasakkers, J. P. Veefkind, TROPOMI ATBD of the total and tropospheric NO2 data products (issue 1.2.0), Royal Netherlands Meteorological Institute (KNMI), De Bilt, The Netherlands, s5P-KNMI-L2-0005-RP (2018).
60. I. De Smedt *et al*., Algorithm theoretical baseline for formaldehyde retrievals from S5p Tropomi and from the QA4ECV Project. *Atmos. Meas. Tech.* **11**, 2395–2426 (2018).
61. W. Sun *et al*., Global significant changes in formaldehyde (HCHO) columns observed from space at the early stage of the COVID-19 pandemic. *Geophys. Res. Lett.* **48**, e2020GL091265 (2021).
62. T. Sherwen *et al*., Global impacts of tropospheric halogens (Cl, Br, I) on oxidants and composition in GEOS-Chem. *Atmos. Chem. Phys.* **16**, 12239–12271 (2016).
63. K. R. Travis *et al*., Why do models overestimate surface ozone in the southeastern United States? *Atmos. Chem. Phys.* **16**, 13561–13577 (2016).
64. R. Lucchesi, File Specification for GEOS-5 FP (Forward Processing), GMAO Office Note No. 4 (Version 1.2). https://gmao.gsfc.nasa.gov/pubs/office_notes. Accessed 1 July 2020.
65. X. Lu *et al*., Exploring 2016-2017 surface ozone pollution over China: Source contributions and meteorological influences. *Atmos. Chem. Phys.* **19**, 8339–8361 (2019).
66. D. B. Millet *et al*., Formaldehyde distribution over North America: Implications for satellite retrievals of formaldehyde columns and isoprene emission. *J. Geophys. Res.* **111**, D24S02 (2006).
67. B. T. Jobson, Y. Huangfu, Impact of cold climates on vehicle emissions: The cold start air toxics pulse. CESTiCC Project 101409. https://cesticc.uaf.edu/research/jobson-airtoxic.aspx. Accessed 1 July 2020.
68. National Bureau of Statistics, The statistics of industrial acticities in January-February 2020 (In Chinese). http://www.stats.gov.cn/tjsj/zxfb/202003/t20200316_1732233.html. Accessed 1 July 2020.
69. R. Gelaro *et al*., The Modern-Era retrospective analysis for research and applications, version 2 (MERRA-2). *J. Clim.* **30**, 5419–5454 (2017).